Electrical Characteristics of XLPE Insulation of High Voltage Cable

OGBOH V. C.[1], ANIONOVO U. E.[2], NWOBU C. C[3], OYIOGU D. C[4], ANIAGBOSO A. O[5]
[1, 2, 3, 4]*Department of Electrical Engineering Nnamdi Azikiwe University, Awka, Anambra State, Nigeria*

Abstract- ***The insulation of high-voltage cables plays a critical role in ensuring reliable power transmission and system longevity. Cross-linked polyethylene (XLPE) has emerged as a preferred insulation material due to its excellent dielectric properties, thermal stability, and mechanical strength. This study investigates the electrical characteristics of XLPE insulation in high-voltage cables, focusing on parameters such as dielectric strength, insulation resistance, partial discharge inception voltage, and breakdown behavior under varying electrical stresses and environmental conditions. Experimental evaluations were conducted using standardized test procedures to assess the performance of XLPE-insulated cables under AC and DC voltages, temperature variations, and moisture exposure. The results indicate that XLPE exhibits high dielectric strength and robust insulation resistance, making it suitable for modern high-voltage transmission systems. Furthermore, the study highlights the effects of aging and thermal stress on the electrical properties of XLPE, providing valuable insights for cable design, maintenance, and fault diagnosis. The findings contribute to the optimization of high-voltage cable performance and the enhancement of power system reliability.***

Keyword: XLPE, Insulation, High-Voltage, Current, Cross-sectional Area, Capacitance, Resistance, Inductance.

I. INTRODUCTION

The demand for polymeric insulating materials in power apparatus such as cables, transformers, motors, and capacitors are growing. Polymers have excellent electrical properties. In addition, good mechanical stiffness, high corrosion resistance, ease of formation, and low cost of manufacturing and maintenance often make them the best choice of insulating materials for many applications. The development of polyethylene in 1941 triggered a dramatic change in the insulation of cables for the transmission and distribution of electrical energy.

Cross-linked polyethylene (XLPE) cable was first patented in 1959 for a filled compound and in 1963 for unfilled by Dr. Frank Percopio. The significantly higher initial-stage cost of such cable slowed its acceptance for utility purposes until 1980s. For transmission class cables (defined as cables operating above 46 kV), as the application of synthetic polymers to cable technology matured, XLPE gradually displaced paper as the insulation material of choice for transmission voltages up to 330 kV. XLPE is the prime extruded material used for transmission cables besides distribution class cables (mostly 15 to 35 kV), although the laminate of paper and polypropylene (PPP or PPLP) has been employed for voltages above 230 kV

II. METHODOLOGY

The following procedure will be followed to achieve the aim and objectives of the research.
(a) Testing of the XLPE Cable at high voltage using Equipment.
(b) Analytical Method analysis of the XLPE Cable at high voltage
(c) Numerical Method analysis of the XLPE Cable at high voltage
(d) Simulation of the XLPE Cable at high voltage using MATLAB/SIMULINK 2018a

3.1.1 Testing of the XLPE Cable at High Voltage using Equipment
As the electric cable is extensively used, one of the issues raised is how to carry out effective tests for cables regularly to ensure the continuity of flow of the power signal.

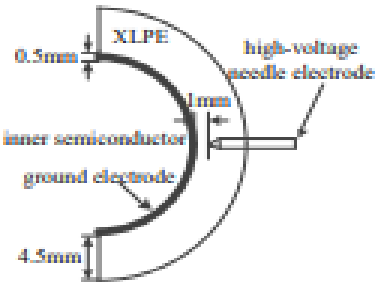

Figure 1: XLPE Cable Specimen

(A) Different Cable Test Methods

The test focuses mainly on the cable insulation layer, the cable leakage, dielectric loss and partial discharge characteristics of cable insulation at low and high voltage conditions. These following methods are to employed for testing the power cable.

(a) M meter method

M meter has many kinds of different voltage stages, including 10kV, 230 kV, 500kV, 1000kV, 2500kV, and 5000kV. The M meter is used to measure the resistance of cable insulation, which reflects the leakage characteristic of cable insulation.

(b) DC Dielectric test

The DC dielectric test reflects the leakage and dielectric characteristics of cable insulation. Both theoretical analysis and practical effect show that the DC or AC dielectric characteristic of oil-filled cable, gas-filled cable, or oil-immersed paper cable is basically the same.

Because the solid dielectric cable such as rubber and plastic cable (including XLPE cable) has sphere gap in the insulation layer, the sphere gap will discharge at DC condition, thus enhancing the dielectric strength. Meanwhile, the back-EMF cannot disappear in time so an accumulative effect forms. When changing applied voltage direction, the dielectric strength reduces significantly. Therefore, the DC dielectric test cannot fully reflect the actual withstand situation of cable, but sometimes do damage to the cables.

When the XLPE cable breaks down during operation, M meter is used to measure the resistance, which is low; DC power source is used to “burn through” the fault, and the insulation resistance becomes higher and higher. In other words, leakage current tends to be normal value and hide the fault. This is because, under the influence of DC, the fault caused by several moisture sphere gaps forms back-EMF after discharging, and dielectric strength is improved, and the conductive bridge is damaged by DC. To conclude, the DC dielectric is not suitable for testing rubber-plastic cable.

(c) Power frequency withstand voltage test

The actual condition of cable insulation is best reflected through the power frequency withstand voltage test. This is because the cable runs at power frequency; its test voltage frequency is proper and theoretically, the power frequency withstand voltage test not only reflects the leakage characteristic of the cable, but also fully reflects partial withstand voltage characteristics caused by dielectric loss.

But in fact, the cable is capacitive load, so there is 150-400pF capacitance per meter. If the length of 10kV XLPE cable is 1km and power frequency test voltage is 20kV, we can calculate the test equipment’s capacity of P = ωCU2 ≮ 50kVA.

Hence, 50kVA voltage regulating controller and 50kVA/20kV test transformer are needed to perform the power frequency test. If the length of the cable is 5km, the equipment capacity is 250kVA. When the cable is too long, the equipment is too heavy to conduct the test.

In order to reduce the volume and weight of the power frequency test device, power frequency series resonant circuit shall be composed of a power transformer, inductance represented by the letter L, and cable, which is shown in Fig.1.

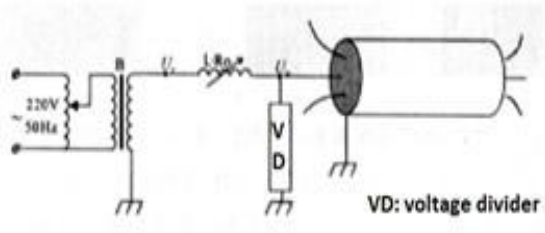

Figure 2: Schematic diagram of power frequency series resonant equipment

The capacitance of the cable is fixed, so the inductance can be adjusted to make the circuit power frequency series resonant. Obviously, this method is better than

the one - directly adopting power frequency transformer to conduct the test. However, the actual equipment is so heavy that you will take trouble operating it.

(d) Super-low frequency (SLF) withstands voltage test
The output frequency of SLF withstand voltage test equipment is generally between 0.01Hz and 0.1Hz. The output waveform is a sine wave or a cosine wave. Hence, the SLF test is also a kind of AC dielectric test. The aim of using the SLF test is to reduce the volume and weight of test equipment as much as possible on condition that the test meets the requirement.

Compared with the power frequency test, the SLF test has many advantages on condition that the test voltage is the same. The capacity of SLF test equipment can be reduced by 50/(0.01-0.1) = 500-5000 times. Other advantages are listed below:

i) possess characteristics of the DC test;
ii) avoid the accumulative effect problem and possess the advantage of power frequency test, that is, detect the insulation problem caused by dielectric loss;
iii) Because the test frequency is low, the insulation reduction is less than that of the power frequency test. Therefore, a dielectric test should be done on-site if possible.

(e) Frequency resonant dielectric test
The capacitance of the cable is certain, so the inductance can be adjusted to make the circuit power frequency resonant. However, it is not easy to tune and the equipment is also very heavy. It is convenient to realize the resonance by means of changing the frequency pf the exciting power source. The frequency ranges from 30Hz to 300Hz.

The variable frequency resonant test system shown in Fig.2 is to reduce the volume and weight of test equipment as much as possible under the condition of equal power frequency test.

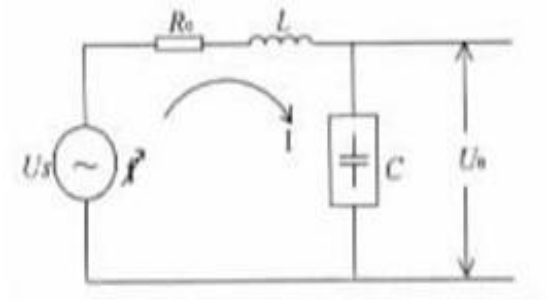

Figure 3: Schematic diagram of variable frequency resonant test

The voltage frequency of the variable frequency resonant test is far higher than the actual working frequency of cable (maximum 6 times). When the frequency is higher, the dipole polarization loss of cable insulation is more serious and it is easier to detect the problem. However, the frequency rises, two and a half conductive layers will intensify the loss of cable.

(f) Dielectric loss measurement of cable
The dielectric loss measurement only reflects the whole condition of cable, involving aging, dampness and loss. The measurement cannot flexibly detect partial degradation and dampness, including cable contact problem. Consequently, it is not suitable for on-site test.

(g) PD test
There are sphere gap and moisture in the insulation of rubber-plastic cable. At rated DC voltage, there is only short-time PD process or no PD at all. At rated AC voltage, the partial discharge may or may not generate. If partial discharge occurs, the process is short. Within certain time partial discharge cannot make cable insulation breakdown but the damage is great. Hence, the PD measurement is performed only for special parts, such as middle contact and terminals.

(h) Oscillation voltage test
The oscillation voltage test is used for the commissioning test of super high voltage cables. In the Fig.3, DC high voltage power source charges the cable; after the cable is fully charged, the switch represented by the letter k is made to “b”; at that time, the cable, inductance and resistance R1 and R2 form series oscillation circuit. The sine wave generates. Whether the cable insulation is good or bad is

determined by measuring some parameters of oscillation waveform. It is easy to use on-site but whether it works still needs to be confirmed.

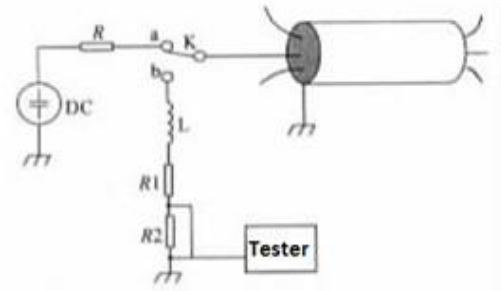

Figure 4: Schematic diagram of oscillation voltage test

As for rubber-plastic cables, the DC dielectric test can only find the phenomenon that cable insulation has obviously degraded or breakdown. It should not be used because it may damage the cable.

The SLF test system is composed of operation control and high voltage power source. It is convenient to operate the device on site and no damage is done to the cables. Hence, it is highly recommended for rubber-plastic cables. At present, the test system is mainly used for ≤35kV cables.

The variable frequency test system is composed of variable power source, exciting transformer, resonant reactor and voltage divider. The variable frequency test system is not suitable for ≤ 35kV cables. It can be used for ≥ 66kV cables.

As for ≥110kV cables, it is easy to conduct the oscillation test on site. But it still needs to be verified whether the effect of oscillation test is as good as SLF test and variable frequency resonant test.

The PD test can only detect special parts of cable (middle contacts and terminals etc). It is necessary to conduct the test on site for those ≥110kV cables. Due to limitations of dielectric loss measurement, it is of no meaning to use it on-site.

III. MODELLING OF ELECTRIC FIELD AND SPACE CHARGE DISTRIBUTIONS IN XLPE 100/ELECTRIC FIELD IN NEEDLE-PLANE ELECTRODE SYSTEM

In polymeric insulated high voltage cables, the treeing phenomenon in the insulation has been identified as an important factor controlling long-term ageing. However, owing to its complicated nature, the mechanisms involved are not yet fully understood. Experimentally, the study of treeing in actual cables is difficult, tedious, time-consuming limited informative and expensive (e.g., actual service voltage or higher is required, tree growth occurs over a long period of time, and the location of trees is random, requiring considerable time for examining sections of the cables). In order to overcome the problems, a method is used whereby a standard defect is introduced into the bulk insulation to mimic the effect of a contaminant or insulation rough surface as found in an actual cable. This "defect" concentrates the electrical stress and serves as an initiation site on which the tree growth is more probable. Moreover, the standard defect gives a controlled, reproducible stress concentration. Generally, there are two kinds of standard defect currently used, i.e., needle-plane and double-needle electrode configurations. These geometries fulfill the requirement of producing high stress intensification (strong divergent stress favours charge injection and tree growth) and repeatable results, such as, typically the characteristic voltage for electrical treeing. Using this technique, it has been shown that electrical trees grow not only under AC stresses but also under DC conditions, voltage ramps, short circuit, polarity reversal and impulse voltages. Charges can be injected by the electrodes under the influence of the electric stress through either Schottky injection or tunnel injection processes. Moreover, hetero-charges can result from the presence of impurities contained within the dielectrics and can generate their own electric stress which is superimposed on the applied electrical stress. It can affect the breakdown stress of the insulating materials in terms of aiding or weakening local electric stress. Recent progress in the non-destructive measurement of space charge distribution in the materials and polymeric cables has had a significant impact on the understanding of electric ageing (including electrical

treeing), high-field conduction and breakdown phenomena.

Three stages are involved in the development of electrical trees, i.e., inception, propagation and completion. Among many experimental setups used to study the treeing phenomena, those allowing inhomogeneous field condition are widely used, and many models have been developed trying to describe the relevant aging process and concomitant partial discharges. It is believed that the tree initiation is the most important phenomenon, since most evidences show that the insulation fails sooner or later once an electrical tree is formed, although this is not an established fact at normally engineering voltages and electric field. It has been reported that large variation in time exists in the first stage of development and is generally attributed to the sample preparation causing morphological difference in the material, or space charge accumulation or experimental conditions such as temperature, or void present at the needle tip. Therefore, special attention should be paid to the local stress variations associated with electrode geometries actually employed in the experimental work. In this chapter, primary studies are carried out firstly on the electric stress profiles of the needle-plane electrode system used for experimental investigation of tree initiation and growth. The effects of diameter of needle, tip angle, tip radius and tip separation on the local electric stress are presented. Based on that, the initiation and propagation mechanisms of electrical treeing are analysed by taking into account the effects of conductive particles, gas bubbles around a conductive particle, and two bubbles, one with space charges inside. Furthermore, regarding the nonlinear conductivity of polyethylene, the electric field and space charge distributions is analysed as well as the influence of voltage waveform. Temperature rise is also calculated by solving an electro-thermal coupling transient problem. Going deeper to macroscopic scale, the space charge accumulation phenomena in insulation bulk is studied based on the bipolar space charge transport model. Since all the developed models are not equivalent because of the lack of enough evidence from current space charge measurements, different assumptions have different explanations for the charge transport phenomena. Two assumptions are applied in the analysis in this project: unique and exponential deep trapping level, respectively.

IV. ELECTRIC FIELD IN NEEDLE-PLANE ELECTRODE SYSTEM

A Analytical Solution of the XLPE Cable at High Voltage

In order to obtain an analytical solution for the needle-plane electrode system, it is assumed that the needle has a hyperbolic shape. The derived formula for the electric stress at the tip of the needle is given by;

$$E_{tip} = \frac{2U(1+\frac{r}{d})^{\frac{1}{2}}}{r\ln(\frac{r+2d+(2d)^{\frac{1}{2}}(d+r)^{\frac{1}{2}}}{r})} \qquad (1)$$

where U is the potential at the needle, r the tip radius of the needle and d the distance between the needle tip and the plane electrode. In the cases where d >> r, the above equation can be further simplified as "Meson's Formula":

$$E_{tip} = \frac{2U}{r\ln(1+\frac{4d}{r})} \qquad (2)$$

The above equation (1) or (2) is widely used to calculate the maximum stress at the needle tip of the XLPE cable. It should be noted that this is the space charge-free "Laplacian" field, which is not relevant to tree initiation, as charge is injected and space charge is formed at high levels (~3000 C/m³) around the tip. In practice, it is very difficult to produce hyperboloid-shaped needles, leading to significant deviations from the ideal shape. The parameters related to needles used for high-voltage insulation material testing vary between laboratories. For example, the needle diameter ranges from 0.685 mm to 1.0 mm; the radius of the needle tip, r, from 1 μm to 100 μm; and the separation distance, d, from 0.5 mm to 10 mm. Additionally, the tip angle is usually 30°. Besides the wide variation in needle geometries, deviations from the hyperboloid shape can cause errors in estimating the actual electric stress using equations (1) or (2). This was not fully understood until recently, when numerical methods revealed different values of electric stress at the needle tip. The finite element method (FEM) has the advantage of geometric flexibility, allowing for a higher density of elements in regions where stress and geometry change rapidly.

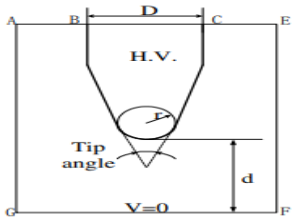

Figure 5: Model used for electric stress computation

3.4.2. Without space charge (ρ = 0)

The highest stress only occurs at the tip of the needle. And the maximum stress at the tip will change with different geometries of the needle. The dependency of the electric stress on the following parameters is studied: D - diameter of the needle; angle of the needle tip; r- radius of the needle tip; d – distance between the needle and the plane. According to chapter four, the variation of electric stress at the needle tip with varying diameters of the needle. It can be seen that the diameter of the needle has little influence on maximum electric stress, especially for the diameter with a higher value. B. An approximately linear relationship is found, and the slope is larger for the needle with a smaller diameter and a steeper tip. C.

A. The influence of needle radius (r)

The variation of electric stress with varying needle radius is shown in Chapter Four. The electric stress at the needle tip, calculated by equation (1) changes dramatically with the change in tip radius. The result by the finite element method also shows the trend. However, the electric stress values obtained from equation (1) are generally higher than the values obtained by finite element method, particularly when the tip radius r < 5 m.

B. The influence of the distance between the needle tip and the plane electrode (d)

In chapter four, the relationship of the electric stress at the needle tip and the distance from the needle tip to the plane electrode. The values obtained from the calculation by equation (1), and finite element method also give a noticeable difference in electric stress. There appears a cross-over point between two curves for two methods, before which the finite element method gives a higher value than equation (1), and after which the finite element method gives a lower value. The difference clearly demonstrates that the hyperbolic shaped needle used in the analytical solution is not a good representation of the needles used in the experimental work.

C. With space charge (ρ ≠0)

It is well known that space charge plays a very important role in dielectric aging and breakdown. Space charge can distort applied fields and to produce locally high fields, leading to dielectric and component aging, and subsequent in-service breakdown, and hence failure, as described earlier in this work. The aging effects are observed in the case of constant stress DC fields, where, over time, a build-up of charge occurs that is either injected homocharge at the electrode-insulator interface or results from deep-trapped bulk charge and possibly void discharge. These effects are a function of the insulation material itself the stress environment conditions such as temperature, impurities, and many other factors. The apparent field necessary for tree initiation at a needle tip, calculated from the applied voltage ignoring space charge, may exceed the breakdown strength of the material by an order of magnitude. Therefore, homocharge must be present around the needle tip, reducing the total effect field to a much lower level. Also, the distinct difference between the tree initiation voltage for a positive and a negative stressed needle attributes to space charge effects. Both electrons and holes are considered to be injected into polymer dielectrics. The time for space charge formation is determined by the dielectric time constant and the rate of change of the applied voltage. Space charge measurement using the pulsed electro-acoustic (PEA) method has shown that the injected charges tend to be trapped reasonably deep in polymeric material used for cable insulation. These deep traps may originate from the interface between crystalline and amorphous regions of the polymer as well as additives. The level of injected space charge is determined by the potential barrier formed at the interface between the electrode and dielectric material. The barrier is governed by the electrophysical properties of the interface such as the work function of the electrode metals or semiconductors, and surface traps of the dielectric. Additives and gas phases may affect the work function and surface traps. The contacts between electrodes and PE are of considerable importance in controlling the amount and distribution of charge in the polymer, and consequently in influencing electrical strength and

aging processes. In the case of PE, it should be emphasized that these contacts can never be uniform on the scale of the polymer morphology. In addition, in the majority of experimental situations, the electrode is metal and covered with oxide or other contact impurities.

In practical situations, such as HV cables, the interface is even more difficult to characterize. However, one needs bear in mind that trapped charge in cables seems to be closely associated with the electrodes. With the assistance of present techniques, space charge injected via the needle electrode now can be measured by several methods. The radius of the space charge boundary R can be derived by using $R = \frac{r(1+\frac{V}{V_c})}{2}$ which is based on the field-limited space charge model, where V is the applied potential and Vc the onset potential for injection. It has been reported that the injecting distance of the space charge into the material varies from 5 to 60μm.

D. The influence of radius of the charge confined spherical region (R)

The extent of the space charge region from the needle tip varies considerably. This may depend on several factors such as the applied voltage, the morphology of the material, temperature, etc. Figure 10 shows the effect of size of the space charge region on the maximum electric stress. The effect on maximum charge density is also illustrated in Figure 10. Although the charge density required to bring the electric stress at the needle tip to zero decreased with increasing charge region, the total charge in this region increased, based on the relationship of $Q = R \cdot q\ 2\pi$.

E. The influence of space charge with reversal polarity (-q)

It has been reported that electrical treeing can be also initiated when the space charge with reversal polarization exists, implying additional high stress may occur due to the presence of space charge. In order to simulate the reversal effect of space charge on electric stress, the sign of the applied voltage or the space charge can be reversed. And the result is shown in Figure 11. Unlike the case of homo-charge, where the maximum electric stress occurs either at the needle tip or the edge of space charge region depending on the charge density, here the maximum electric stress always occurs at the needle tip due to the hetero-charge. And the maximum electric stress with reversal polarization effect is significantly higher than that with homo-charge. The electric stress increases with the increase of either charge density or area of the space charge region (sometimes termed the injecting distance). The maximum stress increases linearly with charge density, with the slope that increases with the increased region size of the injecting charge.

F. The effect of applied voltage (V) on electric stress and charge density

The injection level of space charge is associated with tree initiation voltage in some cases. The relationship between the maximum electric stress and the maximum charge density whose further increase will result in the electric stress at needle tip to be zero via applied voltage, is shown in Figure 12. It is obvious that two linear relationships have been obtained, and the slope may change with a different configuration.

V. THREE CASES OF ELECTRICAL TREE GROWTH

To simulate the distribution of the electric field under the condition of treeing, some parameters were assumed: applied voltage U = 10 kV, the radius of needle tip r = 50 μm or 100 μm, and the distance from needle tip to the ground d = 2 mm. Attempts to simulate electrical tree structures are aimed at elucidating those factors in the propagation dynamics that determine the tree shape [3]. Based on Mason's formula, when d > 10r, the Emax required for the tree growth can be estimated. The Emax has a linear relationship with voltage U for known dimensions. Similar to the results obtained by using the boundary element method (BEM), the electric stress values obtained by equation (1) are generally higher than the values obtained by the FEM method, particularly when the tip radius is less than 5μm. However, as the electrical trees are growing from the needle to the plane electrode, the actual distribution of the electric field would change gradually, considering the conductivity of channels and the effect of space charges. The equivalent circuit method cannot efficiently indicate the details at the microscopic level, and the stochastic model is too complex to separate the influence of each factor from the whole structure. For efficiency and simplicity, the treeing growth model is

abstractly categorized into three cases. They are analyzed here and help investigate the fundamental mechanisms with respect of tree initiation and propagation.

A The Effect of a Conductive Particle

Typical examples for those defects possibly leading to treeing are electrode protrusions (representing the defects at insulating / semiconducting interface in practical, since charge injection from field enhancement tips is shown to be the first step in a series of pre-treeing events.), and floating conductive particles (impurities in insulation bulk as probable tree-initiation locations) as well as the assumed conductive tips of electrical tree channels (due to carbon products cumulated on channel walls, which may result new channel growth combined with space charges or high energy carriers if some conditions are satisfied, e.g. the electromechanical force is high enough to overcome the yield stress of insulating polymer). A needle tip, a conductive particle, or a conductive part of a tree channel can be represented by a conductive or metal ball with tens of micron in radius.

B. Triangular Waveform

In reality, the field at the stress enhancement surface does increase slowly as a function of applied voltage above the critical voltage as the transition between low and high conductivity is not abrupt. If the field distribution is computed accurately using transient nonlinear finite element analysis and realistic models for the field-dependent conductivity even coupled with thermal effect later, the charge on the tip region of a stress enhancement can be determined through application of Guass' Law. In computation, the electric field with space charge effect (Poisson's Equation) is considered as the composition of the Laplace field (Laplace's Equation) and the field induced by space charge. While the space charge-limited field does not increase as a function of the applied voltage, the radius to which the space charge-limited field extends from the stress enhancement does increase with the applied voltage. To analyse the time-dependent effects of rising and falling of applied voltage at the needle tip, similar to the analysis in charging and discharging phenomena, a simple voltage waveform with linearly rising and falling part is considered. Here, it is called "triangular" waveform. This triangular waveform can be defined by

$$V = \frac{V_p}{t_o}.t \qquad 0 \le t < t_o \qquad (3.3)$$

$$V = V_p - \frac{V_p}{t_o}.t - t_o \qquad t_o \le t < 2t_o \qquad (3.4)$$

$$V = 0 \qquad t > 2t_o \qquad (3.5)$$

where Vp is the peak value of applied voltage and 0 t is the transition time of rise part and fall part of the applied voltage. Here, t = 5 ms.

C. AC Waveform

Extending the triangular (unipolar) waveform to the situation of a sequence of continuous sine wave, the AC sine (bipolar) waveform of power frequency is defined by 0 V =Vpsin (2π ft +ϕ) (4-5) where Vp = 40 kV , f = 50 Hz and 0 ϕ = 0 . Applying the AC waveform at the needle tip, when the SCLF is reached, charge starts to be injected from the needle tip into the dielectric. The electric field "pushes" this charge away from the needle tip which causes a force on the dielectric. The force is normally negative, meaning that the force is away from the high field electrode.

D. Temperature Rise

So far, the temperature effect is ignored since the temperature rise is too small to be considered for ms scale waveform because the power frequency scale is long enough for thermal diffusion to limit the temperature rise to lower than 1K for the 5 μm needle tip. Thus, to make the temperature effect become substantial, high frequency waveform is specially applied. Three voltage waveforms have been investigated: a) a step wave with rise time of 10 ns (10% to 90%); b) a step wave with rise time of 100 ns (10% to 90%); and c) a step wave with rise time of 1200 ns (10% to 90%) which is to simulate a standard lightning impulse with a rise time of 1.2 μs (10% to 90%) and a tail of 50 μs (to 50% amplitude). All the three waveforms can be defined by [138]

$$V(t) = \frac{V_p}{2}\left[1 + \tanh\left(\frac{t}{0.45 \times t_r} - 3\right)\right] \qquad (3.6)$$

where Vp is the peak voltage and r t is the rise time in seconds. Here, V_p = 40 kV in order to keep consistent with former computations, and t_{r1} = 10 ns, t_{r2} = 100 ns and t_{r3} = 1200ns and σ (E,T), the electric field E(r,z)is coupled by the temperature T(r,z)through the power dissipation P = J · E .

VI. SIMULATION OF XLPE CABLE

Based on the actual electrical tree sizes shown in Figure 6, a 2D simulation model of electrical tree was constructed in Figure 7. In order to facilitate the research, it was assumed that the central angle of the electrical tree is 120°. Every branch of the electrical tree was 1μm in diameter and 200μm in length in the simulation model. The channels were evenly distributed in the area. In Figure 6, the number of channels was 9 and the angle between adjacent channels was 15°.The depth of needle electrode in insulation was 3.5 mm. The voltage which applied between the needle electrode and the inner semiconductor layer was 6 kV. The inner semiconducting layer was grounded. The electric field distribution of the model was calculated by the finite element method (FEM) to analyses the effect of the number of tree channels.

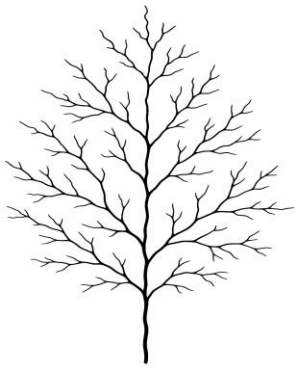

Figure 6: Typical Electrical Tree Shape

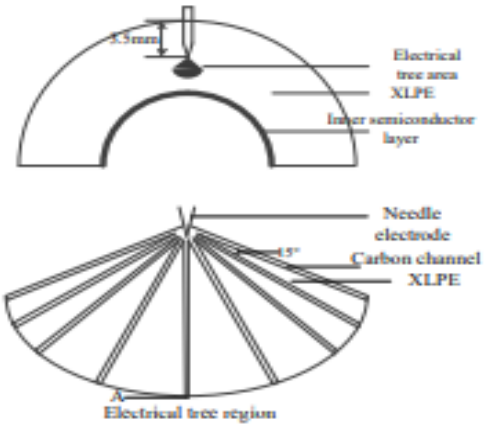

Figure 7: Simulation Model of Electrical Tree Shape

Table 1: Parameters of the Model

S/NO	COMPOSITION	ε_r	$\gamma(S/m)$
1	Steel Needle	0	9.33×10^{6}
2	XLPE	2.3	1.0×10^{-27}
3	Electrical Tree	1	100
4	Semiconductor	20	2.0×10^{-4}
5	Layer		

In order to study the effect of change of branch number on electric field at tip of the tree (A point in Fig 7), the numbers of electrical branches were selected as 1, 3, 5, 9 and whole region was carbonized. The electric field curve with the number of electrical branches at the tip of tree (A point) will be shown on the simulation results.

The simulation result should be able to show level of decrease of the electric field strength at the tip of tree decreased with the increasing number of branches. Based on the Mason formula, the maximum electric field intensity E near the needle tip is given by equations (1) and (2) and determines the if the electrical tree is gradually produced near the tip of the needle or not.

MATLAB/SIMULINK 2018 is used to model the XLPE cable equations (1), (2) and determine the electric field strength of the XLPE cable in accordance with its parameters and properties.

VII. MODELING OF THE ELECTRICAL STRESS EQUATIONS

Awka – Amawbia power distribution line is modeled using their distribution line parameters in MATLAB/SIMULINK.

Also, equations (1) and (2) were modeled using MATLAB/SIMULINK. The two modeled equations were connected to the distribution line with a view of obtaining the analytical values of the electrical stress before and during fault conditions. The graph of electrical stress with the radius and diameter of the XLPE cable explains the relationship between them and the effects of temperature on the XLPE cable. The analysis of the above results is shown on the chapter four. Note that, if the diameter D is far greater than r, then the model subsystem of equation (3.2) will be used to computer the electrical stress on the XLPE cable and vise versa.

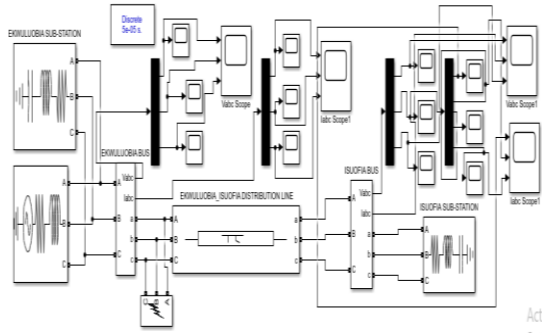

Figure 8: Awka – Amawbia Distribution Line Model

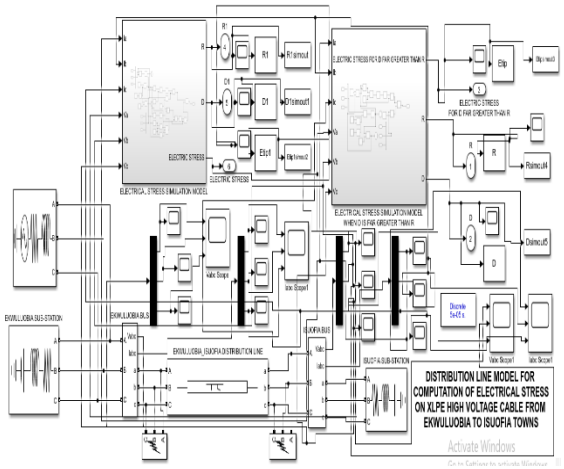

Figure 9: Awka – Amawbia Distribution Line Model with the Electrical Stress Subsystem Models

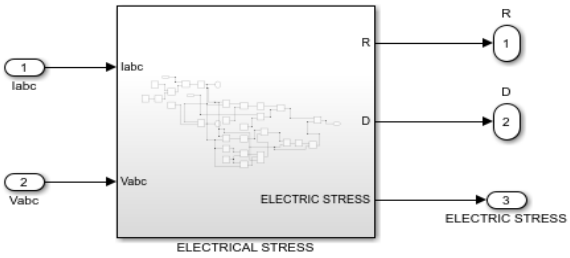

Figure 10: Subsystem Model for the Computation of Electrical Stress when D is not far greater than r.

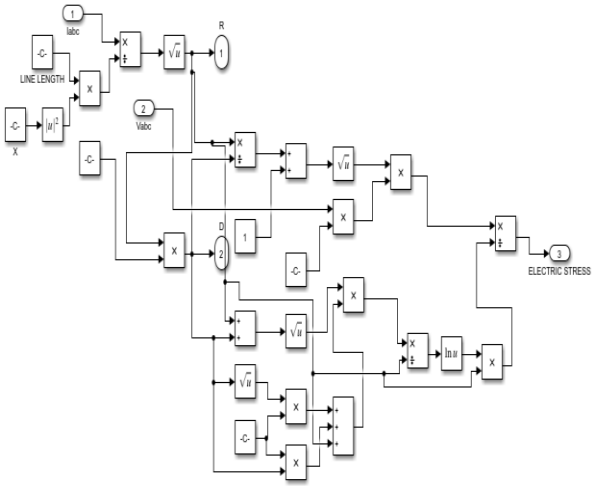

Figure 11: Internal Structure of the Subsystem Model for the Computation of Electrical Stress when D is not far greater than r.

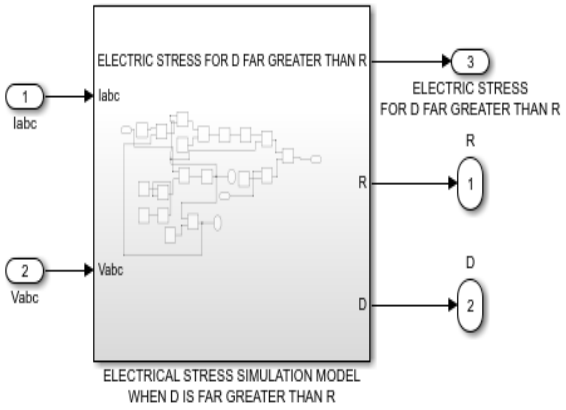

Figure 12: Subsystem Model for the Computation of Electrical Stress when D is far greater than r.

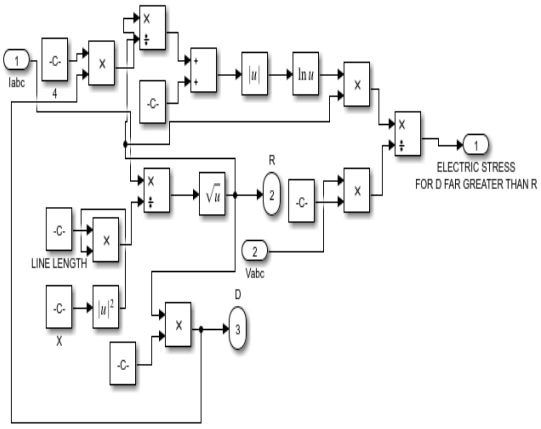

Figure 13: Internal Structure of the Subsystem Model for the Computation of Electrical Stress when D is far greater than r.

VII. RESULTS AND DISCUSSION

A. The Test Report of XLPE Cable

Electrical Type Tests on Completed XLPE Cable
Specimen Description for the Test Conduction

Figure 1: Power Cable of 18/30kV with the following specification:

S/N	ITEM	SPECIFICATION
1	Manufacturer	-
2	Cable Type	18/30KV/AL/XLPE/STA/PVC 3 X 400cm²
3	No of Phases	3 Phase
4	Insulation	XLPE
5	Conduction Material	Aluminum Wires
6	Conduction Cross - Section	400mm²
7	Screening Material	Copper Tape
8	Sheath Material	PVC
9	Sheath Color	Black
	Equipment Description	
10	High Voltage Reactor	400kV – 5000KVA, 50Hz, RSK
11	PD Detector	Type (TE 57)
12	Tan δ measurement device	Type - Dobel M4000
13	Impulse voltage generator	800kv – 40kj, type – ip 40/800m
14	Air oven	300^{0}C, Type BINDER
15	Universal testing machine	100KN – Model LR100KPlus

Bending test, followed by partial discharge test.
Tan δ measurement.
Heating cycle test followed by partial discharge test.
Impulse test followed by a voltage test.
Voltage test for 4 h.
Resistivity of semi-conducting screens.

B. Non-Electrical Type Tests on Cable Components:

A. Measurement of the thickness of insulation
B. Measurement of thickness of non-metallic sheath.
C. Tests for determining the mechanical properties of insulation before and after ageing
D. Tests for determining the mechanical properties of non-metallic sheaths before and after ageing
E. Additional ageing test on pieces of completed cables.
F. Loss of mass test on PVC
G. Hot set test for XLPE insulation.
H. Shrinkage test for XLPE insulation.

VIII. TEST METHOD AND RESULTS:

A. Electrical Type Tests on Completed Cable:

(a) Bending test, followed by partial discharge test:
Bending test: - The test cable was subjected to a bending test at 2500 mm in according with clause 18.2.4. in IEC (60502-2) at ambient temperature for at least one complete turn and unwound without axial rotation. These cycles carried out three times.

Table 2: Bending Test Results on XLPE Cable

S/N	Outer Diameter of Cable D(mm)	Diameter of Conductor d (mm)	Require of Bending Diameter <20(D+d)+5% (mm)	Hub Diameter of Drum (mm)
1	110.00	23.20	2797.00	2500.00

The measured value of the partial discharge level is shown in the following table

Table 3: Partial Discharge Test on XLPE Cable

S/N	Test voltage (kV)	Maximum partial discharge level (PC)	Measured partial discharge level (PC)		
			R	S	T
1	31.00	23.20	1.98	2.16	2.23

Tan δ measurement: Another sample of test cable was subjected to a Tanδ measurement in accordance with clause 18.2.6 of IEC 60502-2. The test cable was heated by passing a current through the conductor until it reached a steady temperature, which was 98 °C. The Tan δ was measured at a power frequency voltage of at least 2 kV at the temperature specified above. The measured value of Tan δ is shown in the following table 4.

Table 4: The measured value of Tan δ

S/N	Test voltage (kV)	Maximum Allowable for Tan δ (x 10^{-4})	Tan δ (x 10^{-4}) [Measured value]		
			R	S	T
1	2.00	40.00	12.00	18.00	20.00

The test results met the requirements.
Heating Cycle followed by partial discharge test:
(b) Heating Cycle:
The test cable was subjected to a heating cycle voltage test in accordance with clause 18.2.7 of IEC 60502-2. The test cable was heated by passing a current through the conductor until it reached a steady temperature, which was 98°C. The heating was applied for 5hrs. The conductor temperature was maintained within the stated temperature limits for 2hrs of each heating period. This was followed by 3 h of natural cooling. The cycle of heating and cooling was carried out 20 times.

Table 5: Results of The Heating Cycle

S/N	Required Conductor Temperature (°C)	Heating		Cooling Time (hr)
		Total Heating Time (hr)	Duration of Heating at 98 °C (hr)	
1	95≤t≤100	5	2	3

(c) Partial discharge test

After the last heat cycle, partial discharge was measured for the test cable at ambient temperature in accordance with clause 18.2.5 of IEC 60502-2. The measurement was carried out as mentioned above under item (1.1.2).

The measured value of the partial discharge level is shown in the following table 4.6.

Table 6: measured value of the partial discharge level

S/N	Test voltage (kV)	Maximum partial discharge level (PC)	Measured partial discharge level (PC)		
			R	S	T
1	31.00	5.00	2.74	2.82	2.91

The test results met the requirements.

(d) Impulse test and voltage test:

Impulse Test: - The test cable was subjected to a lightning impulse voltage withstand test in accordance with clauses 18.2.8 of IEC 60502-2 (2014). The test was performed on the sample at a conductor temperature of 98 °C. The cable withstood 10 positive and 10 negative voltage impulses with peak value of 170 k V without failure.

After the impulse voltage test, the test cable was subjected to a voltage test of was 3.5 U_o. Total voltage was increased gradually to 63kV and maintained for 15 min. in accordance with clause 18.2.8 of IEC 60502-2. - The result of the voltage test is shown in the following table 4.7.

Table 7: Voltage Test Results

S/N	Applied Voltage (KV)	Frequency (Hz)	Duration (mins)	Observation
1	63	50	15	No Breakdown

Voltage test for 4hrs:

The test cable was subjected to the voltage test for 4hrs in accordance with clauses 18.2.9 of IEC 60502-2. This test was made at ambient temperature. A power frequency voltage was applied for 4hrs to the test cable between the conductor and screen. The test voltage was $4U_o$. The voltage was increased gradually to 72kV and maintained for four hours. The result of the voltage test is Shown on table 8.

Table 8: Four Hours (4hrs) Voltage Test Results

S/N	Applied Voltage (KV)	Frequency (Hz)	Duration (hrs)	Observation
1	72.00	50.00	4.00	No Breakdown

The test results met the requirements.

(e) Resistivity of semi-conducting screens:

The measurement of the resistivity of the semi-conducting screens was carried out in accordance with clause 18.2.10 of IEC 60502-2. The resistivity of extruded semiconducting screens applied over the conductor and over the insulation was determined by measurements on test pieces taken from the core of a sample of cable as manufactured and a sample of cable which has been subjected to the ageing treatment to test the compatibility of component materials specified in IEC 60502-2. The measurements were made at a temperature of 90± 2°C.

The result of the Resistivity of semi-conducting screens are shown in the following table 9.

Table 9: The result of the Resistivity of semi-conducting screens

S/N	Item	Unit	Requirement	Measured Value
1	Conductor Screen			
	-without ageing	Ωm	≤ 1000	18.25
	-after ageing	Ωm	≤ 1000	9.87
2	Insulation Screen			
	-without ageing	Ωm	≤ 500	11.67
	-after ageing	Ωm	≤ 500	6.71

The test results met the requirements.

B. Non-Electrical Type Tests on Cable Components:

(a) Measurement of thickness of insulation

The thickness of insulation was measured in accordance with clause 19.2 of IEC 60502-2.

The result of the measurements is shown in the following table 10.

Table 10: The thickness of insulation

S/N	Thickness of Insulation	Unit	Requirement	Measured Value		
				R	S	T
1	Minimum	mm	≥8.00	8.22	8.27	8.35
2	$\frac{t_{max} - t_{min}}{t_{max}}$		≤0.15	0.07	0.07	0.06

The test results met the requirements.

(b) Measurement of thickness of non-metallic sheath:

The thickness of non-metallic sheath was measured in accordance with clauses 19.3 of IEC 60502-2. - The result of the measurements is shown in the following table 11.

Table 11: The thickness of non-metallic sheath

S/N	Thickness of non-metallic sheath	Unit	Requirement	Measured Value
1	Minimum	mm	≥ 3.60	4.30

The test results met the requirements.

(c) Tests for determining the mechanical properties of insulation before and after ageing:

The mechanical properties of insulation before and after ageing were determined in accordance with clause 19.5 of IEC 60502-2.

Table 12: Tests for determining the mechanical properties of insulation before and after ageing

S/N	Item	Unit	Requirement	Measured Value		
1	-without ageing			R	S	T
	Min tensile strength	N/mm²	12.50	20.15	21.74	19.47
	Min elongation	%	200.00	532.14	602.73	392.40
2	-after ageing					
	Min tensile strength	N/mm²	-	18.75	19.07	17.95
	Max variation with samples with ageing	%	± 25.00	-7.04	-12.28	-7.80
	Min elongation	%	-	618.42	684.14	658.10
	Max variation with samples with ageing	%	± 25.00	16.21	13.50	11.09

The test results met the requirements.

Tests for determining the mechanical properties of non-metallic sheaths before and after ageing

The mechanical properties of the outer sheath before and after ageing were determined in accordance with clause 19.6 of IEC 60502-2.

The results of the mechanical properties of non-metallic sheaths before and after ageing are shown in the following table 13.

Figure 13: Results of the Mechanical Properties of Non-Metallic Sheaths before and after Ageing

S/N	Item	Unit	Requirement	Measured Value
1	-without ageing			
	Min tensile strength	N/mm²	12.50	16.78
	Min elongation	%	150.00	231.47
2	-after ageing			
	Min tensile strength	N/mm²	12.50	15.07
	Max variation with samples with ageing	%	± 25.00	-10.19
	Min elongation	%	-150.00	194.97
	Max variation with samples with ageing	%	± 25.00	15.76

The test results met the requirements.

(d) Additional ageing Test on Pieces of Completed Cable:

Ageing tests on pieces of completed cable were carried out in accordance with clause 19.7 of lEC 60502-2 (2014). - The results of the mechanical properties of completed cable are shown in the following table 14.

Table 14: Results of the Mechanical Properties of Completed Cable

S/N	Item	Unit	Requirement	Measured Value		
				R	S	T
1	**Insulation**					
2	-min. tensile strength	N/mm²	12.50	19.01	18.97	2-.14
3	-max. variation with sample ageing	%	**± 25.00**	-5.65	-12.74	3.44
4	Min. elongation	-	200.00	600.10	497.12	556.90
5	Max. variation with sample ageing	%	**± 25.00**	12.77	-17.52	-5.99
6	Sheath					
7	-min. tensile strength	N/mm²	12.50	18.04		
8	-max. variation with sample ageing	%	**± 25.00**	7.68		
9	Min. elongation	%	150.00	192.40		
10	Max. variation with sample ageing	%	**± 25.00**	-16.87		

The test results met the requirements.

(e) Loss of mass test on PVC:

A Loss of mass test on PVC sheath test was carried out in accordance with clause 19.8 of lEC 60502-2.

The results of the Loss of mass test on PVC sheath are shown in the following table 15:

Table 15: Results of the Loss of Mass Test on PVC Sheath

S/N	Thickness of non-metallic sheath	Unit	Requirement	Measured Value
1	Max. loss of mass	Mg/cm²	1.50	1.20

The test results met the requirements.

(f) Hot set test for XLPE insulation: -

A hot set test for the XLPE insulation was carried out in accordance with clause 19.13 of lEC 60502-2. The results of the hot set test for the XLPE insulation are shown in the following table 16:

Table 16: Results of the Hot Set Test for the XLPE Insulation

S/N	Item	Unit	Requirement	Measured Value		
1				R	S	T
	Elongated under load	%	≤175	11.50	124.00	110
2	Permanent elongation	%	≤15.00	6.50	5.30	10.20

The test results met the requirements.

Shrinkage test for XLPE insulation: - A shrinkage test for XLPE insulation was carried out in accordance with clause 19.18ofIEC 60502-2. The result of the shrinkage test for XLPE insulation is shown in the following table 17.

Table 17: The Result of the Shrinkage Test for XLPE Insulation

S/N	Distance L, between marks (mm)	Air oven temperature (°C)	Duration (hr)	Maximum shrinkage (%)	Shrinkage Measurement (%)		
1					R	S	T
	200.00	130.00	1.00	4.00	28.00	31.00	29.00

The test results met the requirements.

However, the power cable ELSEWEDY CABLES 3 x 400 mm² 18/30 kV AL / XLPF/STA/PVC 2017, manufactured by and achieved the requirements of tests mentioned in this report according to lEC 60502-2 (2014). The customer to check of carrying out other remaining tests specified in lEC standard and not included in this report.

B. Analysis of the Analytical results

Equations (1) and (2) has been widely used for the calculation of maximum electrical stress at the needle tip of an XLPE cable. The maximum electrical stress is regarded as the free space charge field. Knowing that the parameters such as the diameter of the needles ∅, radius of the needle tip r and the separation distance d vary from 0.68 – 1.00mm, 1.00 – 100.00μm and 0.50 – 10.00mm respectively.

The angle tip can be used as 30° and if the hyperboloid shape of the needle is not achieved, therefore, it may be regarded as error in the estimation of actual electrical stress using equation (1) or (2).

However, the two equations were modeled using MATLAB/Simulink and were simulated. With the simulation of the equations (1) and (2), the actual electrical stress values on the needle and the waveforms of the parameters will be shown and will explain the relationship between them and the electrical stress during faulty and pre-fault conditions of the XLPE cable.

The following results were obtained and hence their analysis.

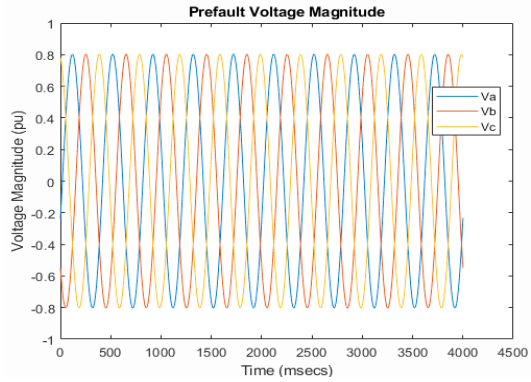

Figure 14: Three phase Pre-fault Voltage Magnitude of the XLPE Cable

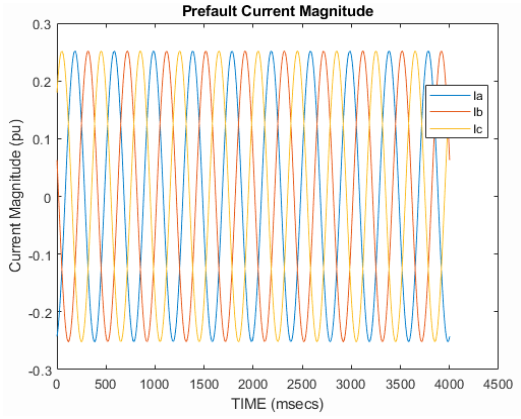

Figure 15: Three phase Pre-fault Current Magnitude of the XLPE Cable

Considering the pre-fault voltage and current magnitude, we can conclude that, the test Ekwuluobia – Isuofia Distribution Network modeled with MATLAB/SIMULINK 2018a is correct, since it gave

accurate graph showing that, the pre-fault voltage is greater than the pre-fault current.

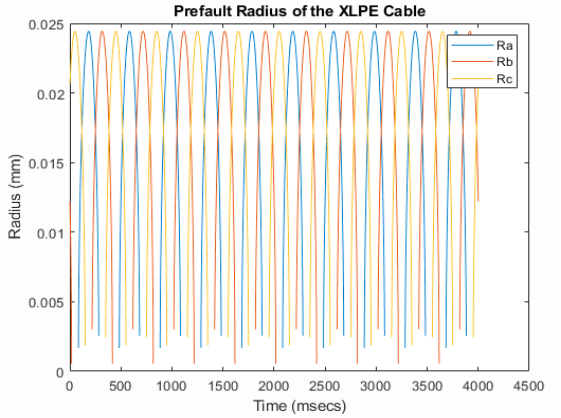

Figure 16: Three phase Pre-fault Radius of the XLPE Cable

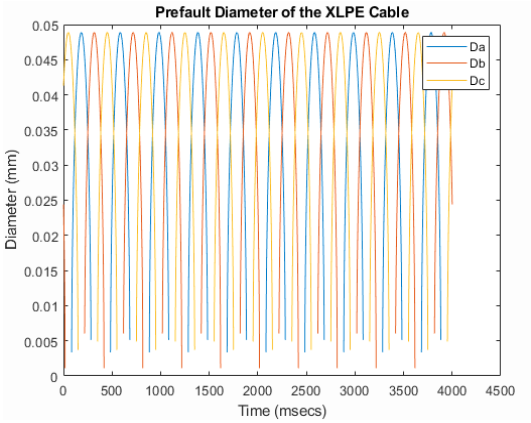

Figure 17: Three phase Pre-fault Diameter of the XLPE Cable

Figures 16 and 17 represent the graph radius and diameter of the XLPE Cable. It is clearly seen on the graphs that; diameter is the twice the radius.

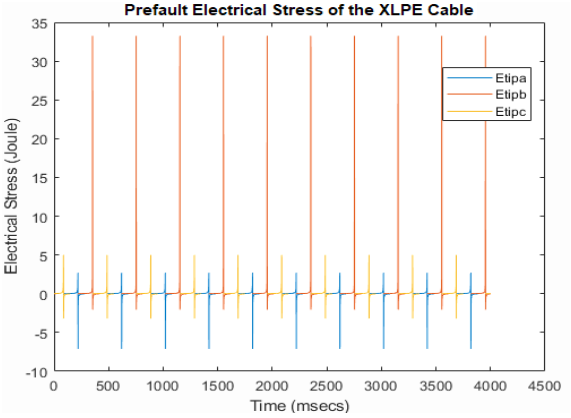

Figure 18: Three phase Pre-fault Electrical Stress of the XLPE Cable

The electrical stress on each XLPE cable on figure 18 vary from each other. This means that, the amount of heat due to stress and current flow on each cable varies.

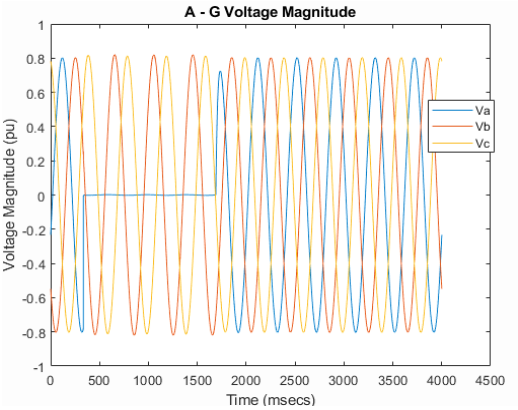

Figure 19: Three phase A – G fault Voltage Magnitude of the XLPE Cable

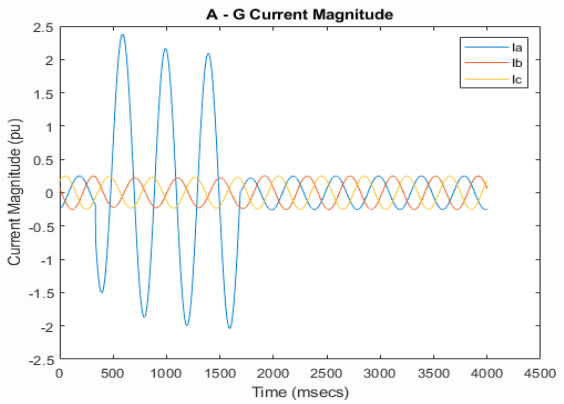

Figure 20: Three phase A – G fault Current Magnitude of the XLPE Cable

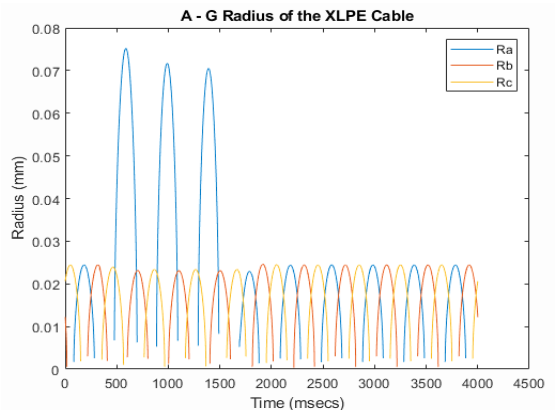

Figure 21: Three phase A – G fault Electrical Stress of the XLPE Cable

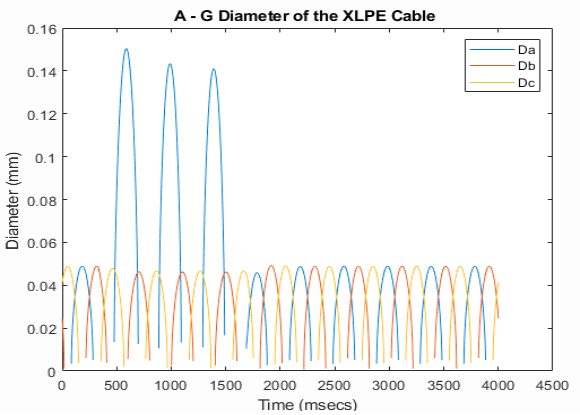

Figure 22: Three phase A – G fault Electrical Stress of the XLPE Cable

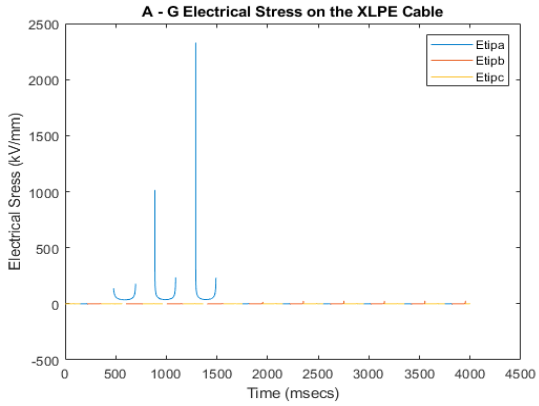

Figure 23: Three phase A – G fault Electrical Stress of the XLPE Cable

At 500, 1000 and 1500 (msecs), Electrical stress on phase A XLPE cable is 100, 1000 and 2200 (joules) respectively. This means that, the amount of heat as a result of fault on that phase was progressively high.

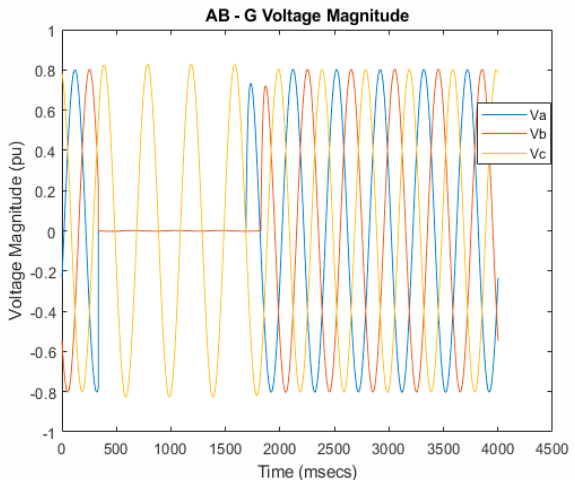

Figure 24: Three phase AB – G fault Voltage of the XLPE Cable

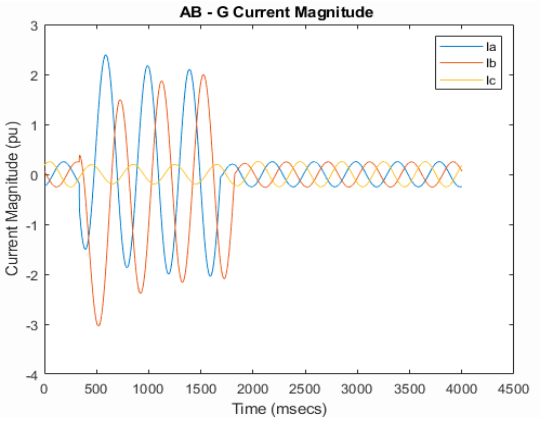

Figure 25: Three phase AB – G fault Current Stress of the XLPE Cable

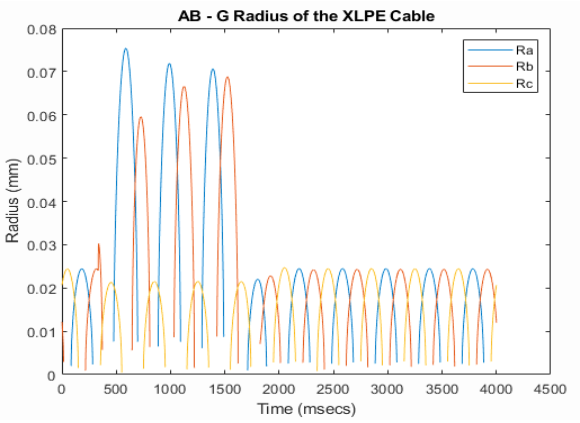

Figure 26: Three phase Pre-fault Electrical Stress of the XLPE Cable

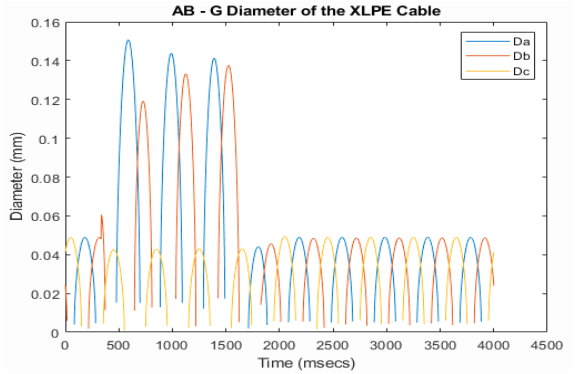

Figure 27: Three phase Pre-fault Electrical Stress of the XLPE Cable

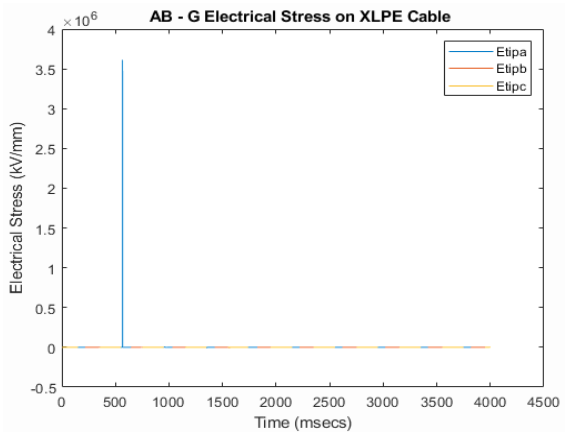

Figure 28: Three phase AB – G fault Electrical Stress of the XLPE Cable

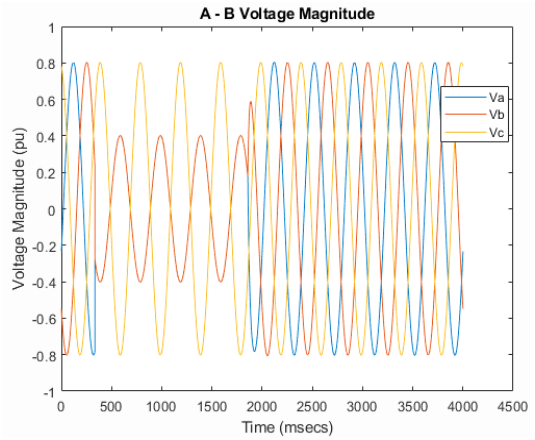

Figure 29: Three phase A – B Fault Voltage Magnitude of the XLPE Cable

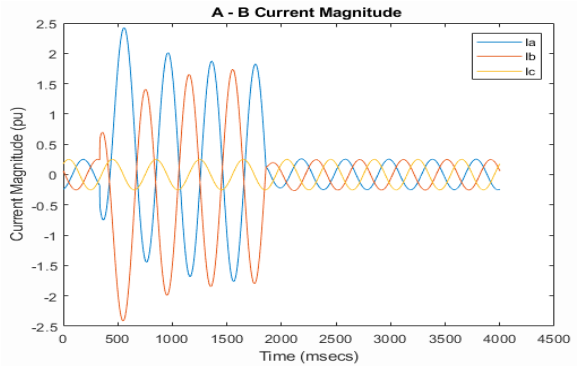

Figure 30: Three phase A – B Fault Current Magnitude of the XLPE Cable

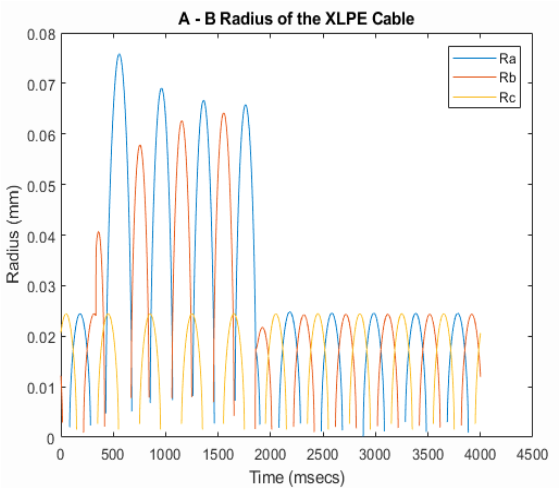

Figure 31: Three phase Pre-fault Electrical Stress of the XLPE Cable

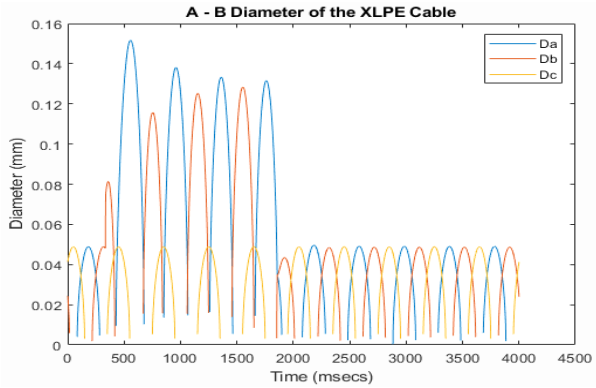

Figure 32: Three phase Pre-fault Electrical Stress of the XLPE Cable

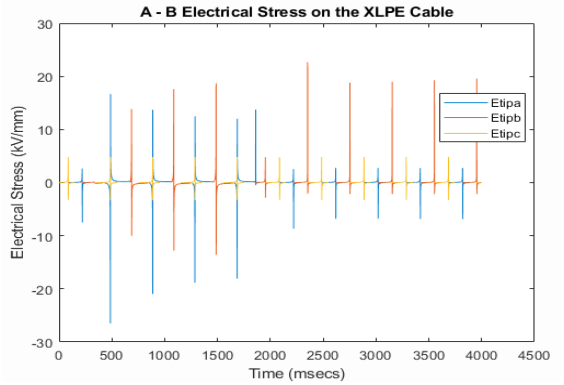

Figure 33: Three phase Pre-fault Electrical Stress of the XLPE Cable

The electrical stress for line-to-line fault is not uniform. This is because of the variation in the effects of the A - B fault current magnitude on the XLPE cable. Remember, increase in the electrical stress is as a result of fault which results in increase in current magnitude, hence increase in temperature of the XLPE cable.

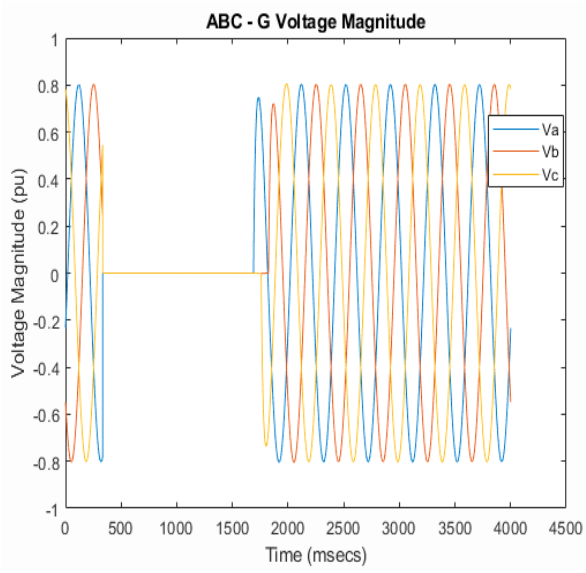

Figure 34: Three phase ABC - G Fault Voltage Magnitude of the XLPE Cable

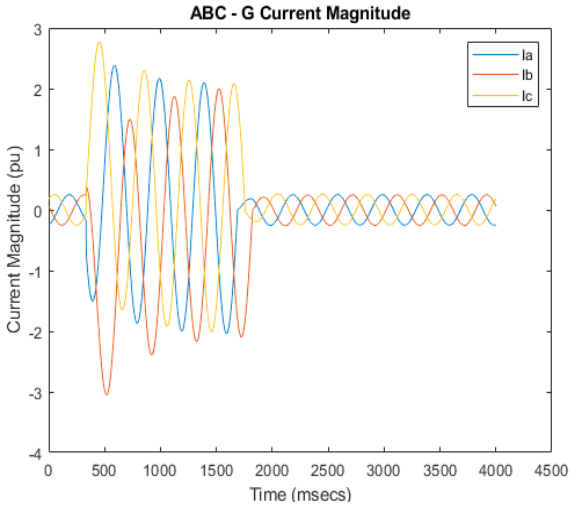

Figure 35: Three phase ABC - G Fault Current Magnitude of the XLPE Cable

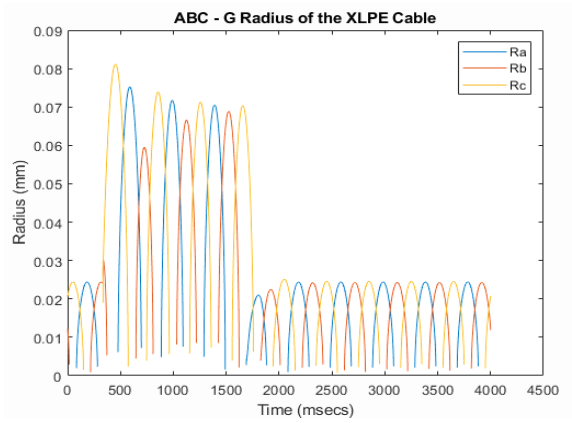

Figure 36: Three phase Pre-fault Electrical Stress of the XLPE Cable

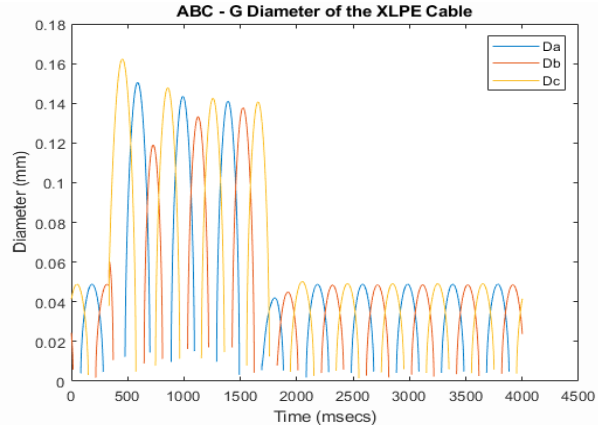

Figure 37: Three phase Pre-fault Electrical Stress of the XLPE Cable

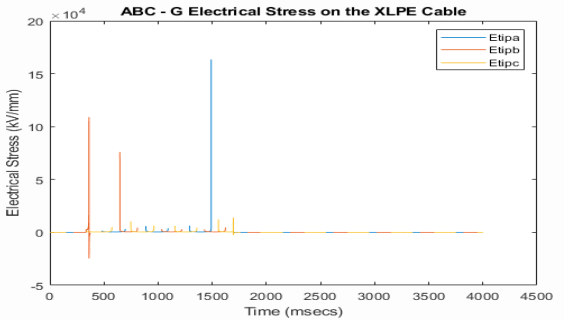

Figure 38: Three phase Pre-fault Electrical Stress of the XLPE Cable

Table 18: Three Phase Pre-fault and Fault Parameters of the Awka – Amawbia Distribution Line

S/N	V_a	V_b	V_c	I_a	I_b	I_c	NETWORK CONDITION
1	0.8000	0.8000	0.8000	0.2500	0.2500	0.2500	PRE-FAULT
2	0.0000	0.8000	0.8000	2.4000	0.2500	0.2500	A – G
3	0.0000	0.0000	0.8000	2.5000	3.0000	0.2500	AB – G
4	0.0000	0.4000	0.8000	2.5000	1.5000	0.2500	A – G
5	0.0000	0.0000	0.0000	2.3000	2.0000	2.8000	A – B – C

Table 19: Three Phase Pre-fault and Fault Parameters of the Awka – Amawbia Distribution Line

S/N	E_{tipa}	E_{tipb}	E_{tipc}	D_a	D_b	D_c	R_a	R_b	R_c	NETWORK CONDITION
1	-7.00	33.00	5.00	0.05	0.05	0.05	0.025	0.025	0.025	PRE-FAULT
2	22.00	0.00	0.00	0.15	0.05	0.05	0.075	0.025	0.025	A – G
3	$3.5X10^4$	0.00	0.00	0.15	0.148	0.04	0.075	0.068	0.020	AB – G
4	-28.00	19.00	5.00	0.15	0.13	0.05	0.075	0.068	0.025	A – B
5	$16x10^4$	$7.8X10^4$	0.00	0.15	0.14	0.16	0.075	0.070	0.080	A – B – C

Again, notice that the fault occurred between 500 milliseconds and 1500 milliseconds. However, electrical stress, radius, and the diameter of the XLPE cable during the A–G fault vary due to an increase in the current magnitude.

8. The effect of applied voltage (V) on electric stress and charge density

The injection level of space charge is associated with the tree initiation voltage in some cases. The relationship between the maximum electric stress and the maximum charge density, whose further increase will result in the electric stress at the needle tip being zero via applied voltage, is shown in Figure 11. It is obvious that two linear relationships have been obtained, and the slope may change with a different configuration.

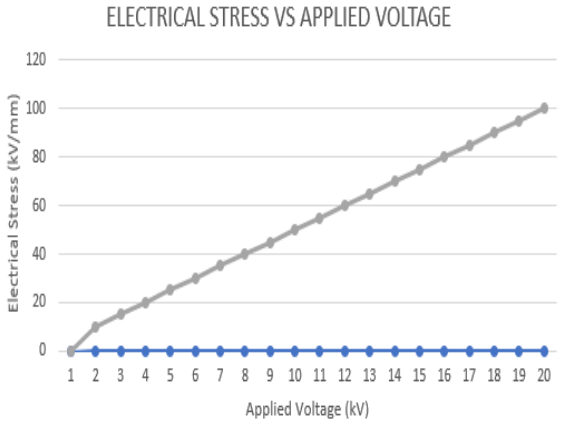

Figure 39: Electrical Stress against Applied Voltage on the XLPE Distribution Cable

The gray line represents diameter while the blue line represents the electrical stress. Considering figure 39, one can easily see the geometrical increase in the value of the electrical stress as the applied voltage increases.

4.4 The influence of needle radius (r)

The variation of electric stress with varying needle radius is shown in Figure 40. The electric stress at the needle tip, calculated by equation (1) changes dramatically with the change in tip radius. The result by finite element method also shows the trend. However, the electric stress values obtained from equation (1) are generally higher than the values obtained by the calculation method, particularly when the tip radius r < 5m.

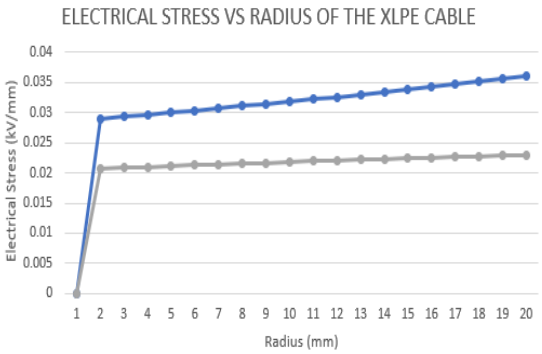

Figure 40: Electrical Stress against Radius of the tip of the XLPE Distribution Cable

The gray line represents diameter while the blue line represents the electrical stress.

4.5 The influence of diameter (D)

Figure 4.28 illustrates the variation of electric stress at the needle tip with varying diameters of needle. It can be seen that the diameter of needle has little influence on maximum electric stress, especially for the diameter with higher value.

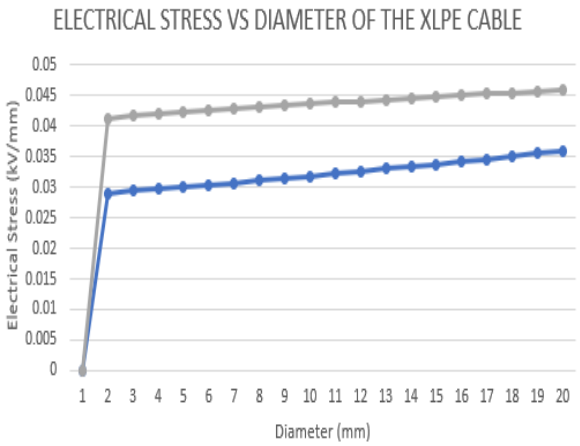

Figure 41: Electrical Stress against Diameter of the XLPE Distribution Cable

The gray line represents the diameter while the blue line represents the electrical stress.

IX. DISCUSSION ON THE RESULTS OBTAINED

The result of test conducted on XLPE cable is shown on tables 1 to 17. These results explain various test types an XLPE cable should undergo.

Bending test shows the required diameter and bending XLPE depending on the applied voltage magnitude. Partial discharge test explains the level of partial discharge that occurs on the XLPE cable when the cable is heated by high current to about $98^{O}C$ for about five hours.

Impulse and voltage test show that, after subjecting the cable to an increase in voltage to check for insulation breakdown, it was observed that, at 72kV, 50Hz, 15hrs, the XLPE cable did not breakdown but still in good shape.

Among other test were non – electrical test such as measurement of thickness of insulation, non – methalic sheath, mechanical properties of insulation, ageing etc.

The simulation results show that, the test distribution line of Awka - Amawbia 11kV modeled in MATLAB/SIMULINK 2018a performed well. This can be seen on the three-phase graph of the pre-fault and faulted voltage and current parameters, which fulfilled the electrical property that states ‘’during pre-fault conditions, the voltage magnitude of the line is always greater than its current counterpart. But, during fault conditions, the voltage drops and current magnitude increases and becomes greater than the voltage. This also reflected on the electrical stress which is directly proportional to the current on the line. Thus, if the current magnitude increases, the electrical stress increases equally due to heat generated by the current increase.

REFERENCES

[1] Muhammad B. Y., Muhammad B. I. ‘’Cable Test and Breakdown Voltage Determination of Joysense Cable Insulation’’. Indonesian Journal of Electrical Engineering and Computer Science Vol. 8, No. 1, October 2017, pp. 177 ~ 183 DOI: 10.11591/IJEECS. Vol. 8. i1. pp177-183.

[2] Tadeusz C., ‘’Conditions of Discharge-Free Operation of XLPE Insulated Power Cable Systems’’.

[3] Ansheng X., Xiaoquan Z., Shengtao L., George C.‘’The Conduction Characteristics of Electrical Trees in XLPE Cable Insulation’’. 16 September 2008; accepted 2 June 2009 DOI 10.10 02/app.30882.

[4] Xiaohuan W., Yang L., Liqun W., Xinzhuo R., Xianjun T. ‘’ XLPE cable health assessment based on Relief-F feature weighted FSVM’’. IOP Conf. Series: Earth and Environmental Science 675 (2021) 012147 IOP Publishing doi:10.1088/1755-1315/675/1/012147.

[5] Xiangrong C., Yang X., Xiaolong C., Gubanski S. M. ‘’ On the Conducting and Non-conducting Electrical Trees in XLPE Cable Insulation Specimens’’. IEEE Transactions on Dielectrics

and Electrical Insulation Vol. 23, No. 1; February 2016.

[6] Liu Y., Zhang S., Cao X., Zhang C. '' Simulation of electric field distribution in the XLPE insulation of a 320 kV DC cable under steady and time-varying states''.

[7] Ramanujam S., Anil K., Awadhesh M. ''Investigation into the failure of XLPE cables due to electrical treeing: A physico chemical approach''. May 2003. Polymer Testing 22(3):313-318. DOI:10.1016/S0142-9418(02)00106-X.

[8] Divya Radha., Jisha S. Lal., K. Asha Krishnan. K. Asha Krishnan., K. S. Devaky. ''General Applications of XLPE Nanocomposites and Blends'' April 2. DOI: In book: Crosslinkable 10.1007/978-981-16- W0486-7-5. Polyethylene Based Blends and Nanocomposites (pp.85-97).

[9] Xiangbing W. ''Influence on Aggregation Structure Changes of Retired Cross-linked Polyethylene (XLPE) Cable Insulation under Pre-Qualification Test''. IOP Conf. Ser.: Mater. Sci. Eng. 585 012049. IOP Conference Series: Materials Science and Engineering.